



## **Reconstruction of depth resolved strain tensor in off-axis single crystals: Application to H + ions implanted LiTaO<sub>3</sub>**

Antonin Louiset, Sylvie Schamm-Chardon, Oleg Kononchuk, Nikolay Cherkashin

### **► To cite this version:**

Antonin Louiset, Sylvie Schamm-Chardon, Oleg Kononchuk, Nikolay Cherkashin. Reconstruction of depth resolved strain tensor in off-axis single crystals: Application to H + ions implanted LiTaO<sub>3</sub>. Applied Physics Letters, 2021, 118 (8), pp.082903. <10.1063/5.0040729>. <hal-03154232>

**HAL Id: hal-03154232**

**<https://hal.science/hal-03154232v1>**

Submitted on 12 Oct 2021

**HAL** is a multi-disciplinary open access archive for the deposit and dissemination of scientific research documents, whether they are published or not. The documents may come from teaching and research institutions in France or abroad, or from public or private research centers.

L'archive ouverte pluridisciplinaire **HAL**, est destinée au dépôt et à la diffusion de documents scientifiques de niveau recherche, publiés ou non, émanant des établissements d'enseignement et de recherche français ou étrangers, des laboratoires publics ou privés.



HAL Authorization

Reconstruction of depth resolved strain tensor in off-axis single crystals: application to  $H^+$  ions implanted  $LiTaO_3$

## Reconstruction of depth resolved strain tensor in off-axis single crystals: application to $H^+$ ions implanted $LiTaO_3$

Antonin Louiset,<sup>1,2</sup> Sylvie Schamm-Chardon,<sup>1</sup> Oleg Kononchuk,<sup>2</sup> and Nikolay Cherkashin<sup>1, a)</sup>

<sup>1)</sup>CEMES-CNRS and Université de Toulouse, 29 rue Jeanne Marvig, BP 94347, 31055 Toulouse Cedex 4, France.

<sup>2)</sup>SOITEC, Parc technologique des Fontaines, Bernin 38926, Crolles Cedex, France.

(Dated: 9 February 2021)

In the context of growing interest in strain engineering, we present a theoretical protocol for the reconstruction of extrinsic and intrinsic strain tensors in single-crystals attached to a template, with an arbitrary oriented coordinate system. Input data for the protocol are extrinsic deformations of lattice planes, i.e. measured with reference to a template. By combining the protocol with elasticity theory, material property modification can be elucidated. Different methods for strain measurements can take advantage of this approach. It has been applied for reconstruction of strain tensor depth distribution in off-axis  $LiTaO_3$  crystal implanted with  $H^+$  ions, which is the key step for piezoelectric thin film-on-insulator fabrication by Smart Cut process. Modifications of composition, lattice parameters and elastic constants are indicated and discussed.

Today, crystalline thin films are widely used in the industry. Investigating strain inside these layers has become a key subject of interest since strain is responsible for various modifications of material properties. In semiconductors, strain enhances carriers mobility<sup>1</sup> and thus performance of Metal-Oxide-Semiconductor Field-Effect Transistors.<sup>2</sup> Strain plays a major role in complex oxide integration in microelectronics. Piezoelectric and ferroelectric crystals are especially of concern thanks to their electro-mechanical and dielectric properties.<sup>3</sup> Direct epitaxial integration of ferroelectric thin films allowed substantial engineering of their spontaneous polarization and Curie temperature.<sup>4</sup> Modern radio frequency front end modules like Temperature Compensated Surface Acoustic Wave filters<sup>5,6</sup> involve Lithium Tantalate ( $LiTaO_3$  or LTO)-On-Insulator ( $SiO_2$ ) (LTOI) substrates<sup>7,8</sup> which are fabricated by film transfer using the Smart-Cut<sup>TM</sup> technology.<sup>9</sup> There, strain gradients are introduced unintentionally during the key process step based on  $H^+$  ions implantation, which should impact LTOI devices performance.

When the  $[0001]$   $c$ -axis is perpendicular to the wafer surface (Z-Cut orientation) and the implanted layer is pseudomorphic to a template, there is only one nonzero out-of-plane strain component of the extrinsic (reference to a template lattice) strain tensor, which can be directly measured.<sup>10</sup> Real devices require off-axis single crystals with the piezoelectric axis tilted away from the normal to the wafer surface and rotated around the  $[\bar{1}\bar{1}20]$  direction.<sup>11</sup> In that case, the surface does not correspond to any crystallographic plane (Fig.1) and nonzero shear strain component appears in such coordinates system. Direct measurement of the out-of-plane and shear strain components is impossible in this system, unless they are reconstructed from measurable deformation of

existing crystalline planes. However, such strain tensor reconstruction, especially as a function of depth, may not be that obvious to obtain and require some approximations.<sup>12</sup>

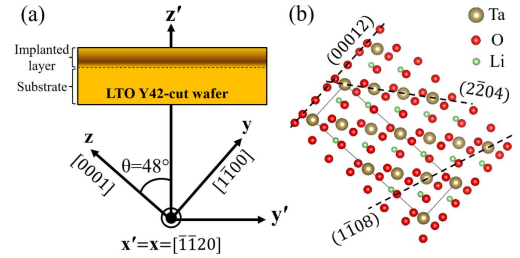


FIG. 1. LTO Y42-Cut viewed along the  $[\bar{1}\bar{1}20]$  direction: (a) Right-handed coordinate systems with crystallographic directions in the implanted wafer and (b) atomic structure and orientation of some studied planes.

Various experimental techniques like Raman spectroscopy,<sup>13</sup> Quantitative Transmission Electron Microscopy (QTEM),<sup>14–17</sup> and X-ray Diffraction (XRD),<sup>18</sup> different in their precision, accuracy and sensitivity to depth distribution, allow the measurement of single plane deformation compared to some reference lattice present nearby. Reconstruction of an extrinsic then intrinsic 2D or 3D strain tensor defined with respect to its own unstrained lattice is a further step, which has not been proposed and challenges a development of dedicated experimental and theoretical protocol.

In this Letter, we present a theoretical protocol for the reconstruction of the extrinsic and intrinsic strain tensors in single-crystals, with an arbitrary oriented coordinate system, by using the measurement of lattice plane extrinsic deformations. The deformation is defined as extrinsic (intrinsic) when the reference and strained materials do not have (do have) the same structure and composition.

<sup>a)</sup>Author to whom correspondence should be addressed: nikolay.cherkashin@cemes.fr

First, we construct reciprocal intrinsic and extrinsic continuum body cells that reflect the corresponding displacement gradients. Any reciprocal vector of the strained material is then expressed in units of intrinsic and extrinsic cells. From the measurement of crystallographic plane extrinsic deformations, we deduce the units of the extrinsic cell, then the coordinates of the strained reciprocal vectors and, finally, the units of the intrinsic cell. The units of the cells are used to calculate the corresponding extrinsic and intrinsic strain tensors.

The protocol is then applied to a practical case, an off-axis LTO 300  $\mu\text{m}$ -thick substrate implanted over 1  $\mu\text{m}$  depth with H<sup>+</sup> ions. Impact of H<sup>+</sup> ions implantation on the LTO properties is considered through the analysis of the extracted strain tensor depth distribution.

Begin by considering the intrinsic Lagrange strain tensor of a material body in real space, for an arbitrary oriented coordinate system  $\mathbf{x}'\mathbf{y}'\mathbf{z}'$ , within the general finite strain theory, i.e. when large shape changes are expected. For the sake of simplicity, we describe the 2D strain tensor, here in the  $\mathbf{y}'\mathbf{z}'$ -plane. First, we choose an unstrained square-like body cell with dimensions  $dy' \times dz'$  and sides parallel to  $\mathbf{y}'$  and  $\mathbf{z}'$  axes. One of its vertices is placed at the coordinate system origin (Fig.2(a), black dashed lines).

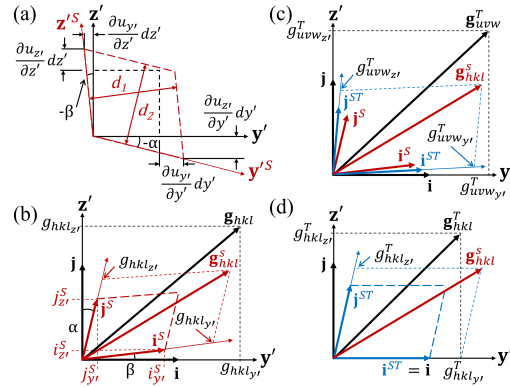


FIG. 2. Unstrained and strained continuum body cells represented: (a) in real space, (b)-(d) in reciprocal space. Unstrained and strained reciprocal lattice vectors represented in units of the continuum body cells: (b) intrinsic case, (c) extrinsic case, (d) a layer pseudomorphic to its substrate. Black, blue and red stand for unstrained, extrinsic strained and intrinsic strained, respectively.

The body is strained when the three other vertices of the cell are displaced in the  $\mathbf{y}'\mathbf{z}'$ -plane by  $\mathbf{u}(\mathbf{y}', \mathbf{z}')$  (Fig. 2(a), red solid lines). The vertex placed on the  $\mathbf{y}'$ -axis is displaced in the  $\mathbf{y}'$  direction by a quantity  $\frac{\partial u_{yy'}}{\partial y'} dy'$  and in the  $\mathbf{z}'$  direction by a quantity  $\frac{\partial u_{yz'}}{\partial y'} dy'$ . The displacements of the vertex placed on the  $\mathbf{z}'$ -axis can be described ac-

cordingly by exchanging  $y', z'$  indexes. The components of the Lagrange strain tensor are then given by the expressions  $\varepsilon_{ij} = \frac{1}{2}(\frac{\partial u_i}{\partial x_j} + \frac{\partial u_j}{\partial x_i} + \frac{\partial u_k}{\partial x_i} \frac{\partial u_k}{\partial x_j})$ , where  $x_i = y'$  and  $x_j = z'$ ,  $\varepsilon_{y'y'}$  is in-plane strain,  $\varepsilon_{z'z'}$  is out-of-plane strain,  $\varepsilon_{y'z'}$  is shear strain. Note that the strained body cell like presented in Fig. 2(a) has a negative shear strain component.

Generally speaking, the strain tensor is deduced from the relative change of the body cell shape and, alternatively, can be described as a function of angles  $\alpha$  and  $\beta$  and relative change in the distances between cell sides, from  $dy'$  to  $d_1$  and from  $dz'$  to  $d_2$  (Fig. 2(a)). From a practical point of view, such a change has to be preferentially introduced in reciprocal space. For this, we construct a reciprocal unstrained body cell with the dimensions  $\mathbf{i} \times \mathbf{j}$  where  $\|\mathbf{i}\| = \|\mathbf{j}\| = 1$  and sides  $i, j$  are aligned along  $\mathbf{y}'$  and  $\mathbf{z}'$  axes (Fig. 2(b)). When strained, the reciprocal body cell obtains the dimensions  $\mathbf{i}^S \times \mathbf{j}^S$  where  $\|\mathbf{i}^S\| = dy'/d_1$ ,  $\|\mathbf{j}^S\| = dz'/d_2$  and  $\mathbf{i}^S, \mathbf{j}^S$  are orthogonal to the  $\mathbf{z}'^S$  and  $\mathbf{y}'^S$  axes, respectively, which are aligned along the sides of the real space strained body cell. Figure 2(b) shows that  $\mathbf{i}^S$  and  $\mathbf{j}^S$  can be expressed in the  $(\mathbf{i}, \mathbf{j})$  reference as

$$\mathbf{i}^S = i_y^S \mathbf{i} + i_z^S \mathbf{j} \quad \text{and} \quad \mathbf{j}^S = j_y^S \mathbf{i} + j_z^S \mathbf{j}. \quad (1)$$

So, one set of reciprocal vectors  $(\mathbf{i}, \mathbf{j})$  describes the unstrained cell and the other  $(\mathbf{i}^S, \mathbf{j}^S)$  the strained one. Note that after real-to-reciprocal space transformation shear strain component inverts the sign. Using this formalism and correcting for the sign of shear strain component, all components of the intrinsic strain tensor can be redefined in reciprocal space as

$$\begin{aligned} \varepsilon_{y'y'} &= \left[ \frac{1}{\|\mathbf{i}^S\|} - 1 \right] + \left[ \frac{1}{2} \left( \left( \frac{1}{\|\mathbf{i}^S\|} - 1 \right)^2 + \left( \frac{i_z^S}{i_y^S} \right)^2 \right) \right], \\ \varepsilon_{z'z'} &= \left[ \frac{1}{\|\mathbf{j}^S\|} - 1 \right] + \left[ \frac{1}{2} \left( \left( \frac{1}{\|\mathbf{j}^S\|} - 1 \right)^2 + \left( \frac{j_y^S}{j_z^S} \right)^2 \right) \right], \\ \varepsilon_{y'z'} &= \left[ -\frac{1}{2} \left( \frac{i_z^S}{i_y^S} + \frac{j_y^S}{j_z^S} \right) \right] + \\ &\quad \left[ -\frac{1}{2} \left( \left( \frac{1}{\|\mathbf{i}^S\|} - 1 \right) \left( \frac{i_z^S}{i_y^S} \right) + \left( \frac{1}{\|\mathbf{j}^S\|} - 1 \right) \left( \frac{j_y^S}{j_z^S} \right) \right) \right]. \end{aligned} \quad (2)$$

The first terms in square brackets approximate the infinitesimal strain tensor valid for deformations which are much smaller than the body dimensions. In order to deduce such intrinsic strain tensor, the 4 coordinates of  $\mathbf{i}^S$  and  $\mathbf{j}^S$  should be determined as a function of measurable quantities. In practice, these are plane deformations determined with respect to a template lattice.

First, one should link the continuum body reciprocal cell  $(\mathbf{i}, \mathbf{j})$  to the periodic reciprocal lattice of the studied material. The latter is composed of reciprocal vectors characterized by proper  $hkl$  indexes and lattice parameters. Let's choose the orthogonal to  $\mathbf{y}'\mathbf{z}'$ -plane, the  $\mathbf{x}'$ -axis, to be parallel to some zone axis of the lattice. Any

reference reciprocal vector  $\mathbf{g}_{hkl}$  perpendicular to that zone axis can be expressed in units of the  $(\mathbf{i}, \mathbf{j})$  cell as

$$\mathbf{g}_{hkl} = g_{hkl_{y'}} \mathbf{i} + g_{hkl_{z'}} \mathbf{j} \quad (3)$$

with  $(g_{hkl_{y'}}, g_{hkl_{z'}}) \in \mathbb{R}^2$  (Fig. 2(b)). When the lattice is strained, this vector becomes  $\mathbf{g}_{hkl}^S$  and is expressed in units of the  $(\mathbf{i}^S, \mathbf{j}^S)$  cell as

$$\mathbf{g}_{hkl}^S = g_{hkl_{y'}} \mathbf{i}^S + g_{hkl_{z'}} \mathbf{j}^S. \quad (4)$$

Assignment of the identical numerical values of  $g_{hkl_{y'}}$  and  $g_{hkl_{z'}}$  in Eqs. (3) and (4) is imposed by the lattice periodicity.

Second, similarly, when the reference is changed to the template material lattice (Fig. 2(c)), the reference reciprocal vector is defined as

$$\mathbf{g}_{uvw}^T = g_{uvw_{y'}}^T \mathbf{i} + g_{uvw_{z'}}^T \mathbf{j}, \quad (5)$$

and the same  $\mathbf{g}_{hkl}^S$  is redefined as a function of vectors  $\mathbf{i}^{ST}$  and  $\mathbf{j}^{ST}$  (the superscript ST stands for "strained" with reference to "template" lattice)

$$\mathbf{g}_{hkl}^S = g_{uvw_{y'}}^T \mathbf{i}^{ST} + g_{uvw_{z'}}^T \mathbf{j}^{ST}. \quad (6)$$

Note that application of such finite strain theory allows different crystal structures for the strained material and that of the template. However, when the strained layer and the template have at least similar structures, the infinitesimal strain is more convenient to apply, because it is linear. In that case,  $\mathbf{g}_{uvw}^T$  must not be too different (in length and direction) to  $\mathbf{g}_{hkl}$ .

Finally, the measurable strain of the  $(hkl)$  plane with reference to the  $(uvw)$  one, the so-called plane extrinsic deformation, is defined by

$$\varepsilon_{hkl}^T = \left[ \frac{\|\mathbf{g}_{uvw}^T\|}{\|\mathbf{g}_{hkl}^S\|} - 1 \right] + \left[ \frac{1}{2} \left( \frac{\|\mathbf{g}_{uvw}^T\|}{\|\mathbf{g}_{hkl}^S\|} - 1 \right)^2 \right] \quad (7)$$

The first term in square brackets describes the plane deformation in the frame of infinitesimal strain theory. By combining Eqs.(1), (5), (6) and (7), it can be written

$$\begin{aligned} \varepsilon_{hkl}^T = & \left[ \frac{\sqrt{g_{uvw_{y'}}^T{}^2 + g_{uvw_{z'}}^T{}^2}}{\sqrt{(g_{uvw_{y'}}^T i_{y'}^{ST} + g_{uvw_{z'}}^T j_{y'}^{ST})^2 + (g_{uvw_{y'}}^T i_{z'}^{ST} + g_{uvw_{z'}}^T j_{z'}^{ST})^2}} - 1 \right] \\ & + \left[ \frac{1}{2} \left( \frac{\sqrt{g_{uvw_{y'}}^T{}^2 + g_{uvw_{z'}}^T{}^2}}{\sqrt{(g_{uvw_{y'}}^T i_{y'}^{ST} + g_{uvw_{z'}}^T j_{y'}^{ST})^2 + (g_{uvw_{y'}}^T i_{z'}^{ST} + g_{uvw_{z'}}^T j_{z'}^{ST})^2}} - 1 \right)^2 \right]. \end{aligned} \quad (8)$$

Accordingly, by using the values of four plane deformations measured with reference to the template, the

four coordinates of  $\mathbf{i}^{ST}$  and  $\mathbf{j}^{ST}$  are determined using Eq. (8). These quantities, when substituted for  $\mathbf{i}^S$  and  $\mathbf{j}^S$  in Eqs. (2), provide the extrinsic strain tensor with reference to a template lattice or, when substituted in Eqs.(6) and equalizing Eq. (4) and Eqs.(6), provide the coordinates of  $\mathbf{i}^S$  and  $\mathbf{j}^S$ . Finally, by substituting the latter into Eqs.(2) one can find the components of the intrinsic strain tensor.

In the following, we present an application of this method for the reconstruction of the depth-resolved strain tensor in off-axis Y42-Cut LTO wafer implanted with  $H^+$  ions at room temperature (RT) at an energy of 110 keV with a fluence of  $9 \times 10^{16} \text{cm}^{-2}$ . This particular off-axis orientation corresponds to the piezoelectric  $c$ -axis being rotated around the  $x=[\bar{1}\bar{1}20]$  direction by  $\theta = 48^\circ$ . We choose the  $\mathbf{x}'\mathbf{y}'\mathbf{z}'$  coordinate system with  $\mathbf{x}'$  parallel to  $[\bar{1}\bar{1}20]$ ,  $\mathbf{z}'$  normal to the wafer surface and  $\mathbf{y}'$  normal to the  $\mathbf{x}'\mathbf{z}'$ -plane (Fig. 1(a)). Secondary Ion Mass Spectroscopy (SIMS) was used to measure hydrogen concentration as a function of depth. Hydrogen is distributed within a 900 nm-thick superficial layer (Fig. 3(b)). High Resolution XRD (HR-XRD) measurements were realized in skew geometry, in order to satisfy Bragg conditions for different  $(hkl)$  reflections. HR-XRD experimental curves were simulated by using RadMax software.<sup>19</sup> One would expect the implanted layer to be pseudomorphic to the substrate and weakly strained similarly to the situation observed for other implanted materials<sup>18,20</sup> and epitaxially grown layers.<sup>21</sup> As a consequence, all crystallographic directions and interplanar distances of the implanted layer should coincide in the  $\mathbf{x}'\mathbf{y}'$ -plane with that of the substrate. Thus, one can set  $\mathbf{i}^{ST} = \mathbf{i}$  and  $\mathbf{g}_{uvw}^T = \mathbf{g}_{hkl}^T$  as represented in Fig. 2(d). That reduces the number of unknown parameters, namely the coordinates of  $\mathbf{j}^{ST}$ , to 2. Using the approximation of infinitesimal strain theory valid for weak strains, Eq. (8) is simplified to a form

$$\varepsilon_{hkl}^T = \frac{\sqrt{g_{hkl_{y'}}^T{}^2 + g_{hkl_{z'}}^T{}^2}}{\sqrt{(g_{hkl_{y'}}^T + g_{hkl_{z'}}^T j_{y'}^{ST})^2 + (g_{hkl_{z'}}^T j_{z'}^{ST})^2}} - 1, \quad (9)$$

which indicates that, in the present application, measurement of only two plane deformations is sufficient for the determination of  $\mathbf{j}^{ST}$ . Note that here  $\mathbf{g}_{hkl}^T = \mathbf{g}_{hkl}^T$  are those of pristine hexagonal LTO (space group:  $R\bar{3}C$ ,  $a^T = 5.1542 \text{ \AA}$ ,  $c^T = 13.783 \text{ \AA}$  measured at RT in this study) with

$$\|\mathbf{g}_{hkl}^T\|^2 = \frac{4}{3} \frac{h^2 + hk + k^2}{a^{T2}} + \frac{l^2}{c^{T2}}. \quad (10)$$

Following the procedure described above, the strain tensor with respect to the template lattice has been determined. First, XRD spectra were obtained for  $\mathbf{g}_{2204}$ ,  $\mathbf{g}_{00012}$  and  $\mathbf{g}_{1108}$  making an angle of  $9^\circ$ ,  $48^\circ$  and  $27^\circ$  with the normal to the wafer surface, respectively. As described in the Supplementary Material, plane deformation profiles along corresponding  $\mathbf{g}_{hkl}^T$  directions were extracted from RadMax simulations and then recalculated as a function of  $\mathbf{z}'$ -depth.

Figure 3(a) shows the resulting  $\varepsilon_{2204}^T(z')$  (red),  $\varepsilon_{00012}^T(z')$  (blue) and  $\varepsilon_{1108}^T(z')$  (green) profiles. The profiles have a similar shape with non zero values at the surface and a maximum value at the same depth of  $\approx 720$  nm.  $\varepsilon_{2204}^T(z')$  and  $\varepsilon_{00012}^T(z')$  were used to calculate  $j_{y'y'}^{ST}(z')$  and  $j_{z'z'}^{ST}(z')$ .

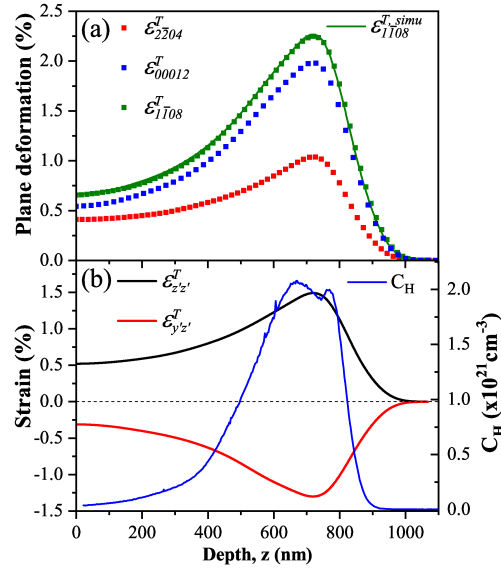


FIG. 3. (a) Plane deformations and (b) strain tensor components with H concentration as a function of  $z'$ -depth obtained for a Y42-Cut LTO wafer implanted with  $H^+$  ions.

We verified our hypothesis of a layer pseudomorphic to the substrate (see Supplementary material) by comparing reconstructed  $\varepsilon_{1108}^{T,simu}(z')$  with that obtained experimentally (Fig. 3(a), green). The very good agreement between these two profiles proves the robustness of the hypothesis and the absence of in-plane plastic relaxation, i.e.  $\varepsilon_{y'y'}^T$  is equal to zero all over the depth.

The remaining unknown components of 2D strain tensor defined with reference to the LTO lattice were then calculated by substituting  $j_{y'y'}^{ST}(z')$  and  $j_{z'z'}^{ST}(z')$  in Eqs. (2). The resulting  $\varepsilon_{z'z'}^T(z')$  and  $\varepsilon_{y'z'}^T(z')$  are plotted in Fig. 3(b). There are gradually changing negative shear strain and tensile out-of-plane strain in the implanted layer. The negative values of  $\varepsilon_{y'z'}^T(z')$  indicate that the body cell is more strongly tensile strained along the  $c$ -axis rather than the  $a$ -axis like shown in Fig. 2(a). Surprisingly, both  $\varepsilon_{z'z'}^T(z')$  and  $\varepsilon_{y'z'}^T(z')$  start with non zero values of 0.5% and -0.3% at the surface, increase in amplitude until reaching a maximum value of 1.5% and -1.3%

at a depth of  $\approx 720$  nm, respectively, then rapidly fall down within a distance of 300 nm. Note that in piezoelectric actuators, strain induced by electric field when exceeding 0.5% is considered giant.<sup>22</sup>

One would expect strain to be directly related to local hydrogen concentration like observed in  $H^+$  ions implanted Si<sup>23,24</sup>. Here, strain profiles being compared to H depth distribution (Fig. 3(b), blue line) only partly support such hypothesis. The depth where strain and H reach their maximum values is the same (the observed peak valley is considered to be a SIMS measurement artifact likely related to the presence of molecular H<sub>2</sub><sup>25</sup>). However, while there is almost no hydrogen near the surface, lattice is still considerably strained there. These data that became accessible only by properly calculating the strain tensor using the analytical model presented in this Letter, strongly support the idea that the implanted layer is no more composed of pristine LTO but of a complex LTO-like alloy with its own gradually changing composition, lattice parameters and elastic constants.

In order to reconstruct intrinsic strain tensor (Eq. (2)),  $a$  and  $c$  lattice parameters of the alloy should be known (Eq. (4)), which is not the case here. To find these parameters, one can combine our protocol with elasticity theory. Stress and strain are related through elastic constants by  $\sigma_{i'j'} = C_{i'j'k'l'} \cdot \varepsilon_{k'l'}$  where  $C_{i'j'k'l'}$  is the fourth order stiffness tensor defined in this particular  $x'y'z'$  coordinate system. In case of in-plane biaxially stressed layer where no force is applied in the  $z'$  direction, the boundary conditions,  $\sigma_{z'z'} = 0$  and  $\sigma_{y'z'} = 0$ , are applied. These two equations link strain components through elastic constants that allows two unknown parameters to be restored. To begin with, we supposed that elastic constants of the alloy equal that of pristine LTO. Within such first order approximation, alloy lattice parameters were calculated. At H maximum concentration,  $a$  is found to be larger by 19% and  $c$  lower by 24.5% than those of pristine LTO. Such differences would impose a drastic change of the implanted LTO structure<sup>26</sup> while it is not confirmed by our X-ray diffraction data. Thus, a change in the elastic constants of the implanted layer should be taken into account as well. Some independent in-plane stress measurements<sup>27</sup> could further reduce the number of unknown parameters. But it comes out of the scope of the present Letter. Anyway, our finding strongly supports the idea that  $H^+$  ions implantation in LTO gradually modifies composition, lattice parameters and elastic constants of the material.

In the context of a growing interest in strain tensor determination in off-axis crystals, in particular, in piezoelectric and ferroelectric materials, we provided an analytical and experimental protocol for the calculation of the 2D finite strain tensor first with reference to a template lattice and then to its unstrained state (intrinsic strain tensor) regardless of crystal orientation. This method requires a measurement of some (maximum 4) plane deformations with reference to a template lattice. The method was applied to successfully reconstruct the



strain tensor depth distribution in  $H^+$  ions implanted off-axis single LTO crystal, with reference to the LTO lattice. Zero in-plane, strong gradually changing negative shear and tensile out-of-plane strain were demonstrated in the implanted layer. Our experiment highlighted a non-direct relation between hydrogen concentration and strain indicating a complex composition and, thus, lattice parameters and elastic constants modification in such piezoelectric material.

The robustness of the approach was approved when applied for prediction of a single plane deformation profile. The method is perfectly compatible with QTEM techniques used for plane deformation measurements.<sup>28</sup> The protocol is applicable to any type of crystalline materials. Finally, the principles of the method can be easily extended for reconstruction of a 3D strain tensor.

#### SUPPLEMENTARY MATERIAL.

See Supplementary Materials [URL will be inserted by publisher] for a more detailed information on XRD experiments and associated RaDMax simulations, as well as a more detailed explanation on the verification of our hypothesis of a layer pseudomorphic to the substrate.

#### ACKNOWLEDGEMENTS

The authors acknowledge useful discussions with Didier Landru from Soitec and Alain Claverie from CEMES. We also would like to thank the Laboratoire de Physique et Chimie des Nano-objets for providing access to XRD facilities (Toulouse, France).

#### DATA AVAILABILITY

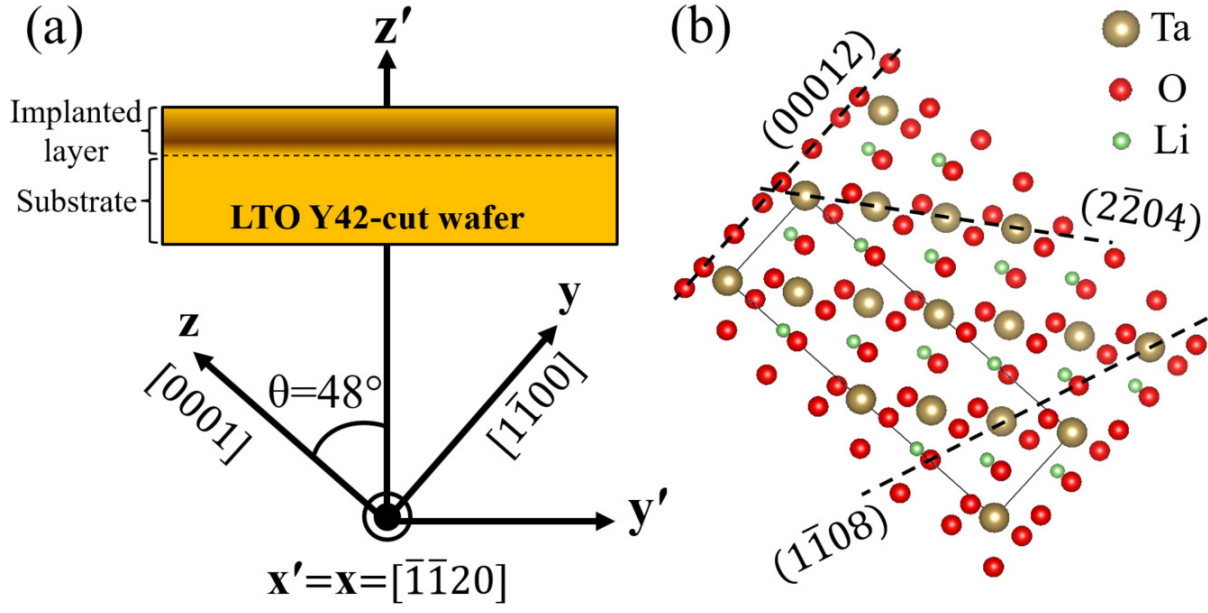
The data that support the findings of this study are available from the corresponding author upon reasonable request.

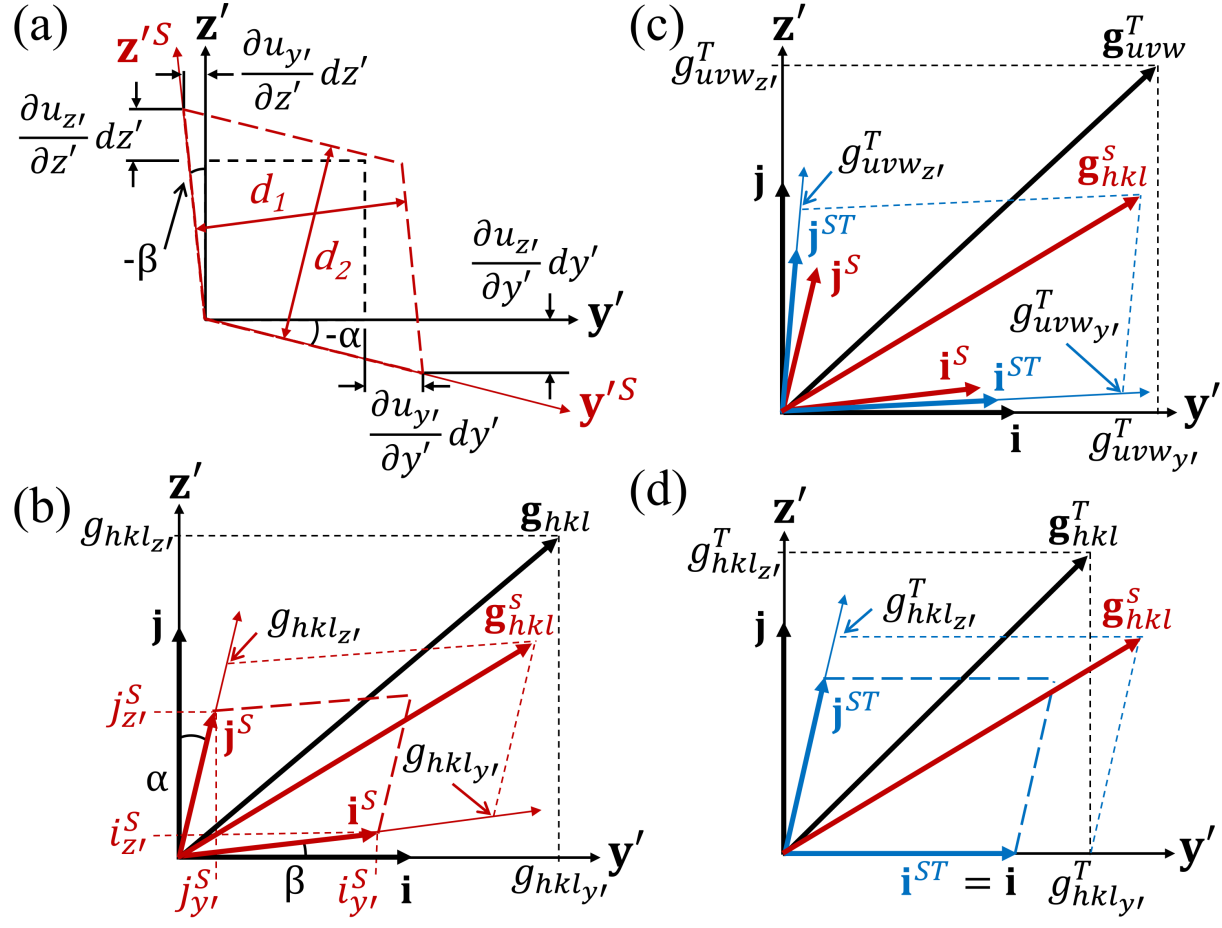
#### REFERENCES

- <sup>1</sup>J. Welser, J. Hoyt, and J. Gibbons, *IEEE Electr. Device L.* **15**, 100 (1994).
- <sup>2</sup>M. L. Lee, E. A. Fitzgerald, M. T. Bulsara, M. T. Currie, and A. Lochtefeld, *J. Appl. Phys.* **97**, 1 (2005).
- <sup>3</sup>P. Murali, R. G. Polcawich, and S. Trolier-McKinstry, *MRS Bulletin* **34**, 658 (2009).
- <sup>4</sup>C. Ederer and N. A. Spaldin, *Phys. Rev. Lett.* **95**, 257601 (2005).
- <sup>5</sup>T. Bauer, C. Eggs, K. Wagner, and P. Hagn, *IEEE Microw. Mag.* **16**, 73 (2015).
- <sup>6</sup>O. Balysheva, in *2019 Wave Electronics and its Application in Information and Telecommunication Systems (WECONF)* (IEEE, 2019) pp. 1–4.
- <sup>7</sup>A. Tauzin, J. Dechamp, F. Madeira, F. Mazen, M. Zussy, C. Deguet, L. Clavelier, J.-S. Moulet, C. Richtarch, T. Akatsu, *et al.*, *Electron. Lett.* **44**, 822 (2008).
- <sup>8</sup>M. Gorisse, A. Drouin, Y. Sinquin, I. Huyet, E. Courjon, F. Bernard, A. Clairet, T. Laroche, M. Bousquet, A. Reinhardt, *et al.*, in *2018 IEEE Intern. Ultrasonics Symposium (IUS)* (IEEE, 2018) pp. 1–4.
- <sup>9</sup>M. Bruel, B. Aspar, and A.-J. Auberton-Hervé, *Jpn. J. Appl. Phys.* **36**, 1636 (1997).
- <sup>10</sup>C. Ma, F. Lu, B. Xu, and R. Fan, *Journal of Physics D: Applied Physics* **49**, 205301 (2016).
- <sup>11</sup>O. Kawachi, S. Mineyoshi, G. Endoh, M. Ueda, O. Ikata, E. Hashimoto, and M. Yamaguchi, *IEEE transactions on ultrasonics, ferroelectrics, and frequency control* **48**, 1442 (2001).
- <sup>12</sup>A. Romanov, T. Baker, S. Nakamura, J. Speck, and E. U. Group, *J. Appl. Phys.* **100**, 023522 (2006).
- <sup>13</sup>F. Pezzoli, E. Bonera, E. Grilli, M. Guzzi, S. Sanguinetti, D. Chrastina, G. Isella, H. Von Känel, E. Wintersberger, J. Stangl, *et al.*, *Mat. Sci. Semicon. Proc.* **11**, 279 (2008).
- <sup>14</sup>A. Béché, J. Rouvière, L. Clément, and J. Hartmann, *Appl. Phys. Lett.* **95**, 123114 (2009).
- <sup>15</sup>N. Cherkashin, T. Denneulin, and M. J. Hÿtch, *Scientific Reports* **7**, 1 (2017).
- <sup>16</sup>M. Hÿtch, F. Houdellier, F. Hÿe, and E. Snoeck, *Nature* **453**, 1086 (2008).
- <sup>17</sup>M. Hÿtch, E. Snoeck, and R. Kilaas, *Ultramicroscopy* **74**, 131 (1998).
- <sup>18</sup>N. Sousbie, L. Capello, J. Eymer, F. Rieutord, and C. Lagahe, *J. Appl. Phys.* **99**, 103509 (2006).
- <sup>19</sup>M. Souilah, A. Boule, and A. Debelle, *J. Appl. Cryst.* **49**, 311 (2016).
- <sup>20</sup>N. Cherkashin, S. Reboh, A. Lubk, M. J. Hÿtch, and A. Claverie, *Appl. Phys. Express* **6**, 091301 (2013).
- <sup>21</sup>J. Bean, T. Sheng, L. C. Feldman, A. Fiory, and R. Lynch, *Appl. Phys. Lett.* **44**, 102 (1984).
- <sup>22</sup>S. Trolier-McKinstry, S. Zhang, A. J. Bell, and X. Tan, *Ann. Rev. Mater. Res.* **48**, 191 (2018).
- <sup>23</sup>N. Cherkashin, F.-X. Darras, P. Pochet, S. Reboh, N. Ratel-Ramond, and A. Claverie, *Acta Materialia* **99**, 187 (2015).
- <sup>24</sup>F. Rieutord, F. Mazen, S. Reboh, J. Penot, L. Bileanu, J. Crocombette, V. Vales, V. Holy, and L. Capello, *J. Appl. Phys.* **113**, 153511 (2013).
- <sup>25</sup>X. Lu, N. W. Cheung, M. D. Strathman, P. K. Chu, and B. Doyle, *Applied physics letters* **71**, 1804 (1997).
- <sup>26</sup>S. Xiang, L. Liu, J. Zhao, X. Zhou, Q. Jing, Y. Zhang, S. Liu, Z. Wang, Y. Bi, H. Geng, *et al.*, *Journal of Physics: Condensed Matter* **25**, 215401 (2013).
- <sup>27</sup>S. Reboh, F. Rieutord, L. Vignoud, F. Mazen, N. Cherkashin, M. Zussy, D. Landru, and C. Deguet, *Applied Physics Letters* **103**, 181911 (2013).
- <sup>28</sup>N. A. Bert, V. V. Chaldyshev, N. A. Cherkashin, V. N. Nevedomskiy, V. V. Preobrazhenskii, M. A. Putyato, B. R. Semyagin, V. I. Ushanov, and M. A. Yagovkina, *J. Appl. Phys.* **125**, 145106 (2019).

This is the author's peer reviewed, accepted manuscript. However, the online version of record will be different from this version once it has been copyedited and typeset.

PLEASE CITE THIS ARTICLE AS DOI: 10.1063/5.0040729







This is the author's peer reviewed, accepted manuscript. However, the online version of record will be different from this version once it has been copyedited and typeset.

PLEASE CITE THIS ARTICLE AS DOI: 10.1063/5.0040729

